Functional Imaging of Oxidative Stress with a Novel PET Imaging Agent, ^{18}F-5-Fluoro-L-Aminosuberic Acid

Jack M. Webster[1], Christine A. Morton[1], Bruce F. Johnson[1], Hua Yang[2], Michael J. Rishel[1], Brian D. Lee[1], Qing Miao[2], Chittari Pabba[1], Donald T. Yapp[3,4], and Paul Schaffer[2]

[1]Diagnostics and Biomedical Technologies, GE Global Research, Niskayuna, New York; [2]Nuclear Medicine Division, TRIUMF, Vancouver, British Columbia, Canada; [3]Division of Pharmaceutics and Biopharmaceutics, Faculty of Pharmaceutical Sciences, University of British Columbia, Vancouver, British Columbia, Canada; and [4]Experimental Therapeutics, BC Cancer Agency, Vancouver, British Columbia, Canada

Glutathione is the predominant endogenous cellular antioxidant, playing a critical role in the cellular defensive response to oxidative stress by neutralizing free radicals and reactive oxygen species. With cysteine as the rate-limiting substrate in glutathione biosynthesis, the cystine/glutamate transporter (system x_c^-) represents a potentially attractive PET biomarker to enable in vivo quantification of x_c^- activity in response to oxidative stress associated with disease. We have developed a system x_c^- substrate that incorporates characteristics of both natural substrates, L-cystine and L-glutamate (L-Glu). L-aminosuberic acid (L-ASu) has been identified as a more efficient system x_c^- substrate than L-Glu, leading to an assessment of a series of anionic amino acids as prospective PET tracers. Herein, we report the synthesis and in vitro and in vivo validation of a lead candidate, ^{18}F-5-fluoro-aminosuberic acid (^{18}F-FASu), as a PET tracer for functional imaging of a cellular response to oxidative stress with remarkable tumor uptake and retention. **Methods:** ^{18}F-FASu was identified as a potential PET tracer based on an in vitro screening of compounds similar to L-cystine and L-Glu. Affinity toward system x_c^- was determined via in vitro uptake and inhibition studies using oxidative stress–induced EL4 and SKOV-3 cells. In vivo biodistribution and PET imaging studies were performed in mice bearing xenograft tumors (EL4 and SKOV-3). **Results:** In vitro assay results determined that L-ASu inhibited system x_c^- as well as or better than L-Glu. The direct comparison of uptake of tritiated compounds demonstrated more efficient system x_c^- uptake of L-ASu than L-Glu. Radiosynthesis of ^{18}F-FASu allowed the validation of uptake for the fluorine-bearing derivative in vitro. Evaluation in vivo demonstrated primarily renal clearance and uptake of approximately 8 percentage injected dose per gram in SKOV-3 tumors, with tumor-to-blood and tumor-to-muscle ratios of approximately 12 and approximately 28, respectively. ^{18}F-FASu uptake was approximately 5 times greater than ^{18}F-FDG uptake in SKOV-3 tumors. Dynamic PET imaging demonstrated uptake in EL4 tumor xenografts of approximately 6 percentage injected dose per gram and good tumor retention for at least 2 h after injection. **Conclusion:** ^{18}F-FASu is a potentially useful metabolic tracer for PET imaging of a functional cellular response to oxidative stress. ^{18}F-FASu may provide more sensitive detection than ^{18}F-FDG in certain tumors.

Several ^{18}F-labeled amino acid derivatives have been used as PET imaging agents to visualize tumors, including *anti*-1-amino-3-^{18}F-fluorocyclobutyl-carboxylic acid, *O*-(2-^{18}F-fluoroethyl)-tyrosine, 6-^{18}F-fluoro-L-dopa, and [18]F-(4R)-4-fluoro-L-glutamine (1–4). These agents rely primarily on the neutral amino acid transporter systems L (large neutral amino acid preferring) and ASC (alanine-serine-cysteine preferring) for tumor uptake (5). By comparison, the most commonly used PET tracer, ^{18}F-FDG, uses an increase in glucose uptake that feeds increased tumor metabolism. Although the molecular mechanisms of glucose and amino acid uptake may differ, they both target augmentations to cellular transport systems that enable higher demands for energy production and protein synthesis required for unrestrained proliferation.

System x_c^- was first described by Bannai and Kitamura as a sodium-independent amino acid transport system with a very narrow natural substrate binding profile (6,7), especially when compared with other known transporters (8). This cystine/glutamate transporter is a dimeric cell surface transporter that consists of a heavy chain subunit (4F2hc) for membrane trafficking and xCT, the smaller subunit that imparts substrate specificity. The xCT subunit maintains very low basal expression in most normal tissues, with the exception of the brain, pancreas, spleen, and thymus, but is universally upregulated as cells respond to oxidative stress (9). The ubiquitin-ligase protein KEAP1 acts as a biosensor for oxidative stress through a reactive oxygen species–induced covalent modification of an active site cysteine residue. Modified KEAP1 can no longer facilitate the proteasomal degradation of the transcription factor Nrf2, resulting in the expression of several genes with antioxidant response element (ARE) promoters, including xCT (10–13) as shown in Figure 1. The resulting enhanced cystine influx, and intracellular reduction to cysteine, meets the increased demand for this rate-limiting precursor of glutathione synthesis. Therefore, system x_c^- imaging can provide functional information about the cellular response to oxidative stress in a tumor or organ, operating as an in vivo reporter for ARE activation.

Targeting system x_c^- for PET tracer development has potential advantages over other amino acid transporters. First, detection of
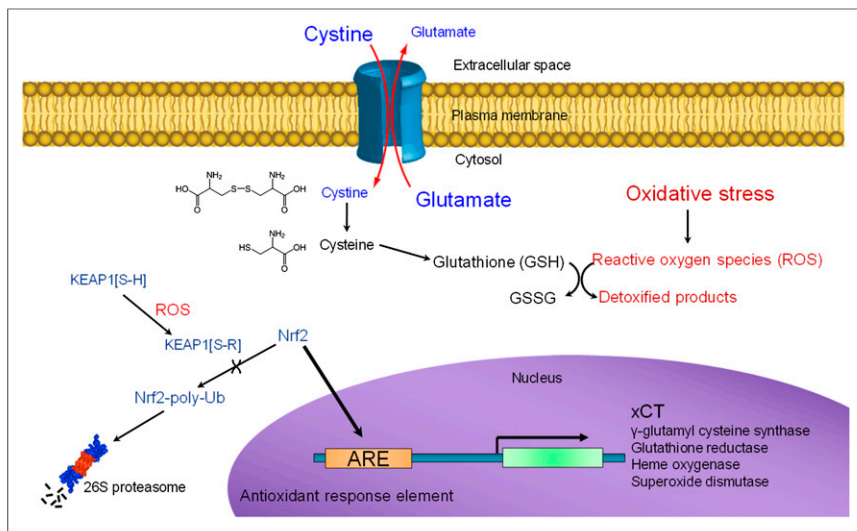
FIGURE 1. Cellular mechanism of xCT expression induced by oxidative stress and promoting increased glutathione synthesis.

oxidative stress distinguishes this biomarker from cell growth and proliferation-based imaging agents. Second, xCT is accessible at the cell surface and maintains a well-defined (and narrow) natural ligand complement, suggesting that PET tracers can be developed with much better selectivity for this class of transporter. Most amino acid–based PET agents use transport systems ASC or L, which transport 14 of the 20 standard amino acids (5), and many of these amino acids are also substrates for several other molecular transport systems. Of the standard amino acids, only L-glutamate (L-Glu) and L-cystine are substrates for system x_c^-, and far fewer additional transport systems use either of these substrates (9), most notably L-Glu as a substrate for the excitatory amino acid transporter of system X_{AG}^- (10,11). Finally, use of an accumulatory transport mechanism could also serve to improve PET signal contrast through enhanced tracer uptake, compared with saturable binding of an agent to a cell surface protein.

Two groups have reported radiolabeled L-Glu derivatives [18]F-(4R)fluoro-L-glutamate (^{18}F-FGLU) and (4S)-^{18}F-fluoropropyl-L-glutamate (^{18}F-FSPG) as PET agent substrates of the cystine/glutamate transporter for cancer imaging (3,14–16). Here, we report evaluation of a series of anionic amino acids of varying carbon chain lengths to identify the best inhibitor of system x_c^-, synthesis of the novel radiofluorinated derivative ^{18}F-5-fluoro-L-aminosuberic acid (^{18}F-FASu), and preclinical evaluation in tumor xenografts. Our efforts to develop a PET imaging substrate of system x_c^- focused on amino acid derivatives that show molecular similarities to the natural uptake substrate, L-cystine. We reasoned that the longer carbon backbone of L-aminosuberic acid (L-ASu) was more cystine-like and may be a better transporter substrate because L-cystine was reportedly more potent toward system x_c^- than L-Glu (9). In addition, cystine-like derivatives may be less likely to participate as substrates for other glutamate transporters or bind to glutamate receptors (17), potentially resulting in better specificity of ^{18}F-FASu in peripheral tissues and the brain (18). The cystine/glutamate transporter is often active in oncology (9,10); using this transporter to image a cellular response to oxidative stress may provide functional information useful for clinical cancer care, such as detection, staging, patient stratification, monitoring of response to therapy, and development of new therapies.

MATERIALS AND METHODS

L-aspartic acid (L-Asp), D-aspartic acid (D-Asp), L-Glu, L-leucine (L-Leu), L-serine (L-Ser), suberate, sulfasalazine (SSZ), 2-aminobicyclo-(2,2,1)-heptane-2-carboxylic acid (BCH), and diethylmaleate were obtained from Sigma. L-aminoadipic acid, DL-aminopimelic acid, and L-aminosuberic acid (L-ASu) were obtained from Bachem. ^{3}H-L-glutmate (^{3}H-L-Glu) and ^{3}H-L-Leucine (^{3}H-L-Leu) were purchased from American Radiolabeled Chemicals. L-aminoazelaic (L-AAz), L-aminosebacic acid, and L-amino 4,5-^{3}H-suberic acid (^{3}H-L-ASu) were synthesized as described in the supplemental data (supplemental materials are available at http://jnm.snmjournals.org).

Radiosynthesis of ^{18}F-FASu

The synthesis of ^{18}F-FASu was independently performed at both GE Global Research and TRIUMF, with efforts at GE Global Research focusing on a radiopharmaceutical preparation method involving high-performance liquid chromatography (HPLC). TRIUMF, along with the BC Cancer Agency, focused on a SepPak (Waters)-based purification method, avoiding the use of HPLC altogether. Detailed descriptions of each group's experimental protocols are provided in the supplemental data. Briefly, ^{18}F-FASu was prepared from the tosylate precursor using a 2-step anhydrous [18]F− nucleophilic displacement strategy as shown in Figure 2.

Cell Culture Experiments

The human ovarian carcinoma cell line SKOV-3 and murine lymphoma cell line EL4 were obtained from the American Type Tissue Collection and cultured according to vendor recommendations. Cells were maintained in T-75 culture flasks in a humidified incubator at 37°C and 5% CO_2 and routinely passaged at confluence. Tumorigenic cell lines were chosen for in vitro and in vivo studies. EL4 cells were chosen to provide large rapidly growing tumors with potential for assessment in immunocompetent animals (for future studies). SKOV-3 cells were chosen to provide slower-growing tumors with more control over tumor size and relevance to human disease.

SKOV-3 cells were subcultured into 12- or 96-well culture-treated plates and grown to confluence. Cells were incubated with 100 μM diethylmaleate 24 h before the uptake assay. Cells were washed with a 4-(2-hydroxyethyl)-1-piperazineethanesulfonic acid–buffered Hanks Balanced Salt solution (HBS). ^{3}H-L-Glu, ^{3}H-L-ASu, ^{3}H-L-Leu, or ^{18}F-FASu was added in the absence or presence of a 1 mM concentration of test compound. For 12-well plate assays, 0.74 kBq (20 nCi) per well was delivered in a 500-μL volume (or 0.037 MBq [1 μCi] per well for ^{18}F-FASu). For 96-well plate assays, 7.4 kBq (200 nCi) per well were delivered in a 50-μL volume. Cells were washed 3 times after the uptake incubation period with HBS. For 96-well plate assays, the last wash was aspirated, 200 μL of Microscint 20 (Perkin Elmer) were added to each well, and the plate was analyzed with a TopCount microplate scintillation counter (PerkinElmer). For 12-well plate assays, cells were solubilized by the addition of 1 mL of 1M NaOH. For uptake in EL4 cells, equal numbers of diethylmaleate-treated cells were aliquoted into microcentrifuge tubes and washed 2 times with HBS by centrifugation. Cell pellets were resuspended in HBS containing ^{18}F-FASu in the absence or presence of inhibitor compounds, incubated while rocking at room temperature for 30 min. Cells were washed 2 times with fresh HBS, and cell pellets were resuspended in 500 μL of 1M NaOH. Solubilized samples with tritium were trans-
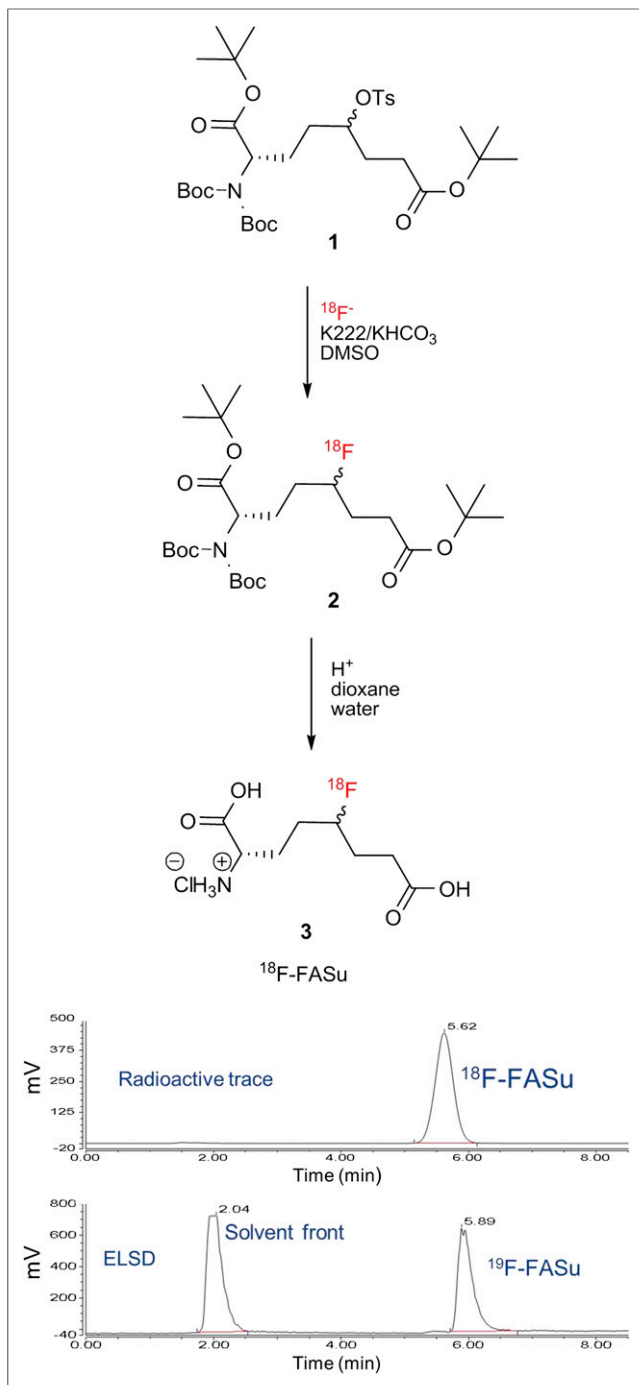
FIGURE 2. 2-step radiosynthesis and identification of ^{18}F-FASu. HPLC of final product with γ detector demonstrates more than 98% radiochemical purity. HPLC of ^{19}F-FASu standard with evaporative light scattering detector (ELSD) shows that differences in retention time of peaks matches 0.27-min (16-s) delay between the 2 detectors.

ferred to a vial with 12 mL of scintillation cocktail and analyzed with a Tri-Carb scintillation counter (Perkin Elmer). For ^{18}F-FASu assays, solubilized cells were added to vials and analyzed using a Wizard γ counter (Perkin Elmer).

Small-Animal PET and Biodistribution Studies

CD-1 nude mice were purchased from Charles River Laboratories, and Rag2-M mice were bred in-house at the BC Cancer Agency.

Animals were housed under sterile conditions with food and water ad libitum and a 12-h light cycle. Mice were injected subcutaneously with 1×10^7 EL4 or SKOV-3 cells in phosphate-buffered saline or culture medium while under 2% isoflurane anesthesia, and tumors were allowed to grow for approximately 5–10 or 21 d, respectively. All animal studies were performed in accordance with federal and Institutional Animal Care and Use Committee guidelines using approved protocols.

For biodistribution studies, mice bearing EL4 tumor xenografts were injected via the tail vein with between 0.07 and 0.59 MBq (2–16 μCi) of ^{18}F-FASu. Direct comparison of ^{18}F-FASu and ^{18}F-FDG involved a cohort of 10 nude mice bearing SKOV-3 tumors randomly separated into 2 groups of 5; each group was injected with approximately 0.44 MBq (12 μCi) of either ^{18}F-FASu or ^{18}F-FDG. Mice were euthanized by CO_2 asphyxiation at the postinjection time points indicated, and then blood was collected by cardiac puncture and organs were excised, weighed, and counted on a γ counter. All urine was collected on filter paper and counted with the bladder. The unused tissues and remaining carcass were collected and counted. The percentage injected dose per gram (%ID/g) was calculated using the sum of the counts from all tissues, urine, and carcass as the injected dose value.

For PET imaging studies, CD-1 nude mice bearing SKOV-3 tumors were injected with 8.5–11.1 MBq (230–300 μCi) of ^{18}F-FASu via the tail vein. PET imaging data were acquired with an eXplore VISTA preclinical PET scanner (GE Healthcare) under 2% isoflurane anesthesia. Static PET data conducted at 1 h (±5 min) after injection were acquired over 10 min (55–65 min after injection) using 2 bed positions. Mice were then immediately euthanized while under anesthesia by cervical dislocation, and an ^{18}F biodistribution evaluation was performed as described above. Images were reconstructed, and region-of-interest analysis was performed on the tumor. The injected dose for imaging studies was determined with a dose calibrator (Capintec). % ID/g and standardized uptake value were calculated using a scaling factor determined by analysis of an equivalent acquisition of a dose-calibrated ^{18}F-FASu standard.

Alternatively, Rag2-M mice bearing EL4 tumors were anesthetized (2% isoflurane), a 27.5-Ga catheter intravenous line containing saline was placed into the tail, and the rodent was positioned on the scanner imaging bed with integrated heating pad (Inveon; Siemens). Each PET scan was initiated using between 4.5 and 16.4 MBq (122–444 μCi) of ^{18}F-FASu in no more than 125 μL of saline administered via the intravenous line. PET data were collected in list-mode for up to 2 h after injection of the tracer. Scan data were then reconstructed with correction from CT-based attenuation, and regions of interest were placed on the tumor and organs of interest to evaluate the time–activity curves for ^{18}F-FASu in the tissues of interest.

RESULTS

In Vitro Cell Uptake Studies

The inhibition of ^{3}H-L-Glu uptake in SKOV-3 cells determined for anionic amino acids ranging from 4 carbons (C_4) to 10 carbons (C_{10}) is shown in Figure 3A. L-Leu and suberate were also examined as negative control compounds. A specific system x_c^- nonsubstrate inhibitor, sulfasalazine, was used as a positive control. The results show that the 5-carbon L-Glu inhibits ^{3}H-L-Glu uptake via the x_c^- transporter by 83%. As the carbon chain is extended to 6-, 7-, or 10-carbon atoms in length, the inhibition of ^{3}H-L-Glu uptake is reduced to between 40% and 70%. However, the 8-carbon compound L-ASu and the 9-carbon derivative L-AAz demonstrate inhibition of ^{3}H-L-Glu uptake similar to L-Glu at 85% and 79%, respectively. The best inhibitors appear to have a distance between the 2 terminal carboxyl groups (in a fully extended conformation)
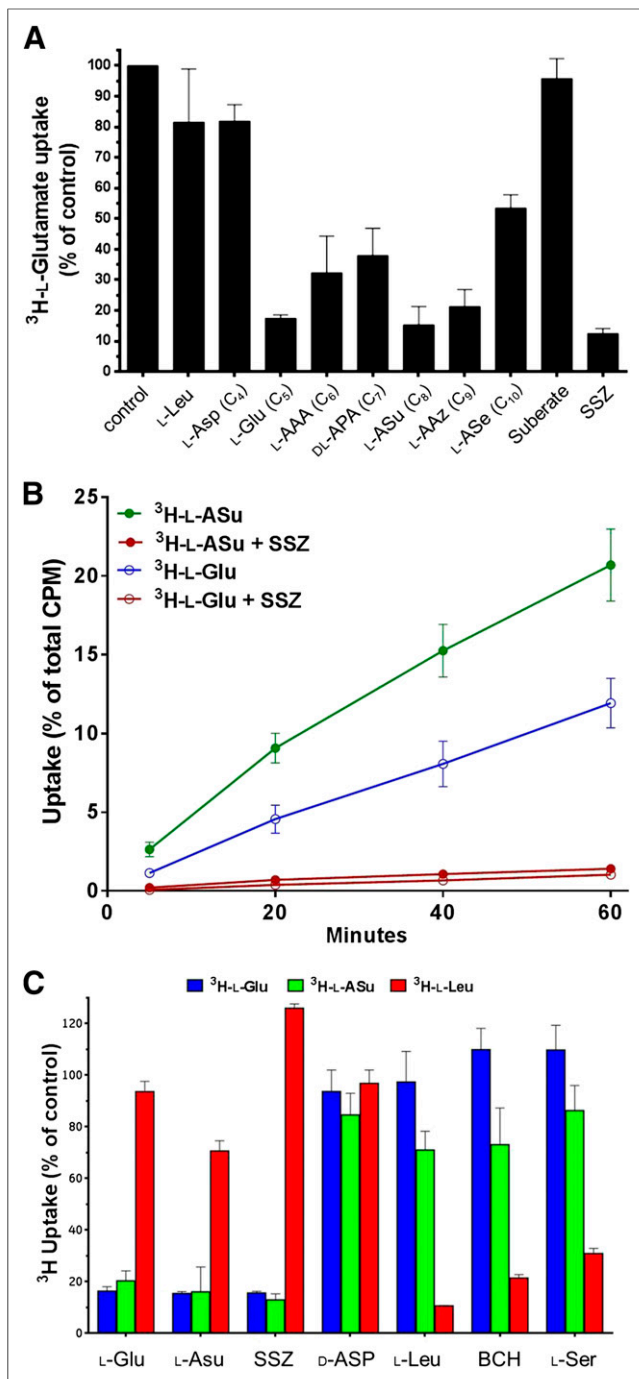
FIGURE 3. In vitro system x_c^- inhibition, uptake, and specificity studies in diethylmaleate-treated SKOV-3 cells. (A) Competitive inhibition of test agents on ^{3}H-L-Glu uptake during 30-min incubation. L-Asp, L-Glu, L-aminoadipic acid, DL-aminopimelic acid, L-ASu, L-AAz, and L-aminosebacic acid are all anionic amino acids from 4 to 10 carbons (C_4–C_{10}) in length, respectively. Values are normalized to uptake of ^{3}H-L-Glu in phosphate-buffered saline alone (mean ± SD, $n = 3$). (B) Comparison of direct cell uptake of ^{3}H-L-ASu and ^{3}H-L-Glu. ^{3}H-L-ASu and ^{3}H-L-Glu were matched for specific activity and radiation dose per sample. Uptake values are expressed as percentage of total activity used per well (mean ± SD, $n = 3$). (C) Comparison of ^{3}H-L-Glu, ^{3}H-L-ASu, and ^{3}H-L-Leu uptake in presence of selected amino acid transporter inhibitors for 30 min. ^{3}H-L-Glu, ^{3}H-L-ASu, and ^{3}H-L-Leu were matched for specific activity and radiation dose per sample. Values are normalized to uptake of each agent in phosphate-buffered saline alone (mean ± SD, $n = 3$). SSZ = sulfasalazine.

that best approximates the distances in the natural substrates L-Glu (5.0 Å, C_5) and L-cystine (9.8 Å, between C_8 and C_9). Negative controls suberate and L-Leu, as well as the 4-carbon L-Asp, showed less than 20% inhibition of ^{3}H-L-Glu uptake.

A comparison of direct uptake of ^{3}H-L-ASu and ^{3}H-L-Glu in SKOV-3 cells is shown in Figure 3B. ^{3}H-L-ASu uptake was 2.3, 2.0, 1.9, and 1.7 times more than the uptake of ^{3}H-L-Glu at 5, 20, 40, and 60 min, respectively. These results suggest that while competitive inhibition results were similar, L-ASu appears to be a more efficient transporter substrate, resulting in better in vitro uptake. Uptake of ^{3}H-L-ASu and ^{3}H-L-Glu was inhibited 92.6% and 92.1%, respectively, with 500 μM sulfasalazine, suggesting that most uptake of these agents can be attributed to the x_c^- transporter.

To evaluate specificity of L-ASu for the system x_c^- transporter, we measured the uptake of ^{3}H-L-Glu, ^{3}H-L-ASu, and ^{3}H-L-Leu in the absence and presence of inhibitors (Fig. 3C). Inhibitors used included the system x_c^- inhibitor sulfasalazine; the excitatory amino acid transporter inhibitor D-Asp; transport systems L, B^0, and B^{0+} inhibitor L-Leu; transport system L inhibitor BCH; and systems A, ASC, B^0, and B^{0+} inhibitor L-Ser. Results demonstrate less than 20% uptake relative to controls for ^{3}H-L-Glu and ^{3}H-L-ASu in the presence of L-Glu, L-ASu, and sulfasalazine, with little, if any, effect on uptake in the presence of L-Leu, BCH, and L-Ser. An inverse relationship was noted for ^{3}H-L-Leu, demonstrating more than 80% uptake in the presence of L-Glu, L-Asu, and sulfasalazine and pronounced inhibition with the latter 3 inhibitors. D-Asp had little inhibitory effect on all tracers.

Radiosynthesis and Uptake of ^{18}F-FASu

Both GE Global Research and TRIUMF used a 2-step nucleophilic displacement strategy for the synthesis of ^{18}F-FASu (Fig. 2) but proceeded to tracer formulation with and without HPLC purification, respectively. Decay-corrected yields were between 5% and 15%, with more than 98% radiochemical purity as determined by peak integration of the corresponding analytical HPLC traces, and were dependant on the experimental protocol. The radiochemical purity of the final product after isolation was more than 98%, regardless of the synthetic method used.

The uptake of ^{3}H-L-ASu and ^{18}F-FASu were both inhibited in EL4 cells by L-ASu and L-Glu (Fig. 4A), suggesting that ^{18}F-FASu is also a substrate for the system x_c^- transporter. ^{18}F-FASu was assayed for cell uptake in cultured SKOV-3 cells (Fig. 4B) and showed nonsaturable uptake over 1 h, which is potently inhibited to between 7% and 16% of control by sulfasalazine, consistent with uptake via system x_c^-. Because system x_c^- activity and ^{18}F-FASu uptake were observed in these in vitro models, we decided to evaluate uptake and imaging in EL4 and SKOV-3 subcutaneous xenograft tumors in vivo.

^{18}F-FASu In Vivo Biodistribution and Imaging Studies

In vivo biodistribution studies were first performed in CD-1 nude mice bearing subcutaneous EL4 xenograft tumors. The clearance of ^{18}F-FASu in mice is shown in Figure 5A. Renal clearance predominates because most activity is quickly partitioned to the kidney, bladder, and urine. Tracer continued to accumulate in the bladder and urine and to clear from blood, kidneys, liver, and spleen over the course of 4 h. Figure 5B shows that EL4 tumor uptake is significant and remains fairly constant up to 2 h after injection. Evaluation of ^{18}F-FASu tissue distribution at 1 h after tail vein injection is shown in Table 1, with tumor-to-blood
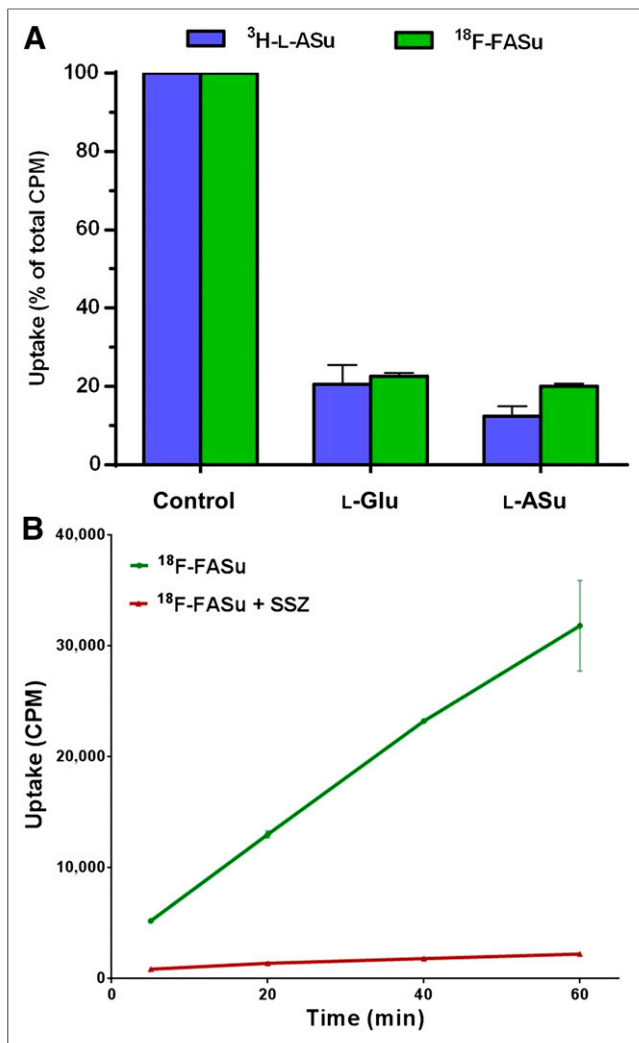
FIGURE 4. Uptake of HPLC-purified ^{18}F-FASu in EL4 and SKOV-3 cells in vitro. (A) EL4 cells were evaluated for uptake of ^{3}H-L-ASu and ^{18}F-FASu in absence or presence of 1 mM L-Glu or L-ASu for 30 min. Uptake and inhibition profiles were similar for both radiolabeled compounds. Values are normalized to uptake of each agent in phosphate-buffered-saline-alone control (mean ± SD, $n = 4$). (B) ^{18}F-FASu uptake in SKOV-3 cells in absence and presence of 0.5 mM sulfasalazine was evaluated with 5-, 20-, 40-, and 60-min incubations. Uptake values are raw CPM values per sample (mean ± SD, $n = 3$). SSZ = sulfasalazine.

ratios of approximately 12 and tumor-to-muscle ratios of approximately 28. ^{18}F-FASu also demonstrated prominent retention in the pancreas and significant retention in the spleen.

We conducted a side-by-side comparison of ^{18}F-FASu and ^{18}F-FDG in CD-1 nude mice bearing SKOV-3 tumors at 1 h after injection (Table 1); we chose the SKOV-3 cells for this study because their slow growth allowed for more control over tumor size. ^{18}F-FASu tumor uptake at 1 h after injection reached 8.1 %ID/g, with tumor-to-blood and tumor-to-muscle ratios of approximately 12 and approximately 30, respectively. As expected, ^{18}F-FASu also showed pronounced uptake in the pancreas and spleen. ^{18}F-FDG tissue distribution is also shown in Table 1. Compared with ^{18}F-FDG, ^{18}F-FASu showed a 5.2-fold-greater tumor uptake and a 4.6-fold-greater tumor-to-blood ratio. ^{18}F-FASu also demonstrated much lower background in muscle, heart, and brain.

CD-1 nude mice bearing SKOV-3 tumor xenografts were injected with ^{18}F-FASu by tail vein, and PET imaging was conducted 1 h after injection (Fig. 6). Tumor uptake obtained by necropsy biodistribution evaluation of the mouse immediately after imaging, 8.4 %ID/g, correlated well with the mean tumor uptake analysis from the PET image, 8.6 %ID per cubic centimeter (%ID/cm^3). Maximum pixel intensity in the tumor was 16.7 %ID/cm^3. The mean standardized uptake values of the tumor were 2.5 and 4.9, respectively. Imaging results were consistent with SKOV-3 biodistribution data shown in Table 1.

Dynamic PET images of EL4 tumors in Rag2-M mice (Fig. 7A) revealed a rapid and high initial tumor uptake exceeding 6 %ID/cm^3 by 40 min after injection, staying close to this level for the 2-h duration of the scan (Fig. 7B). A high tumor-to-muscle ratio of approximately 13 at 120 min after injection was also indicative of a low overall background uptake of the tracer. Uptake in the kidneys
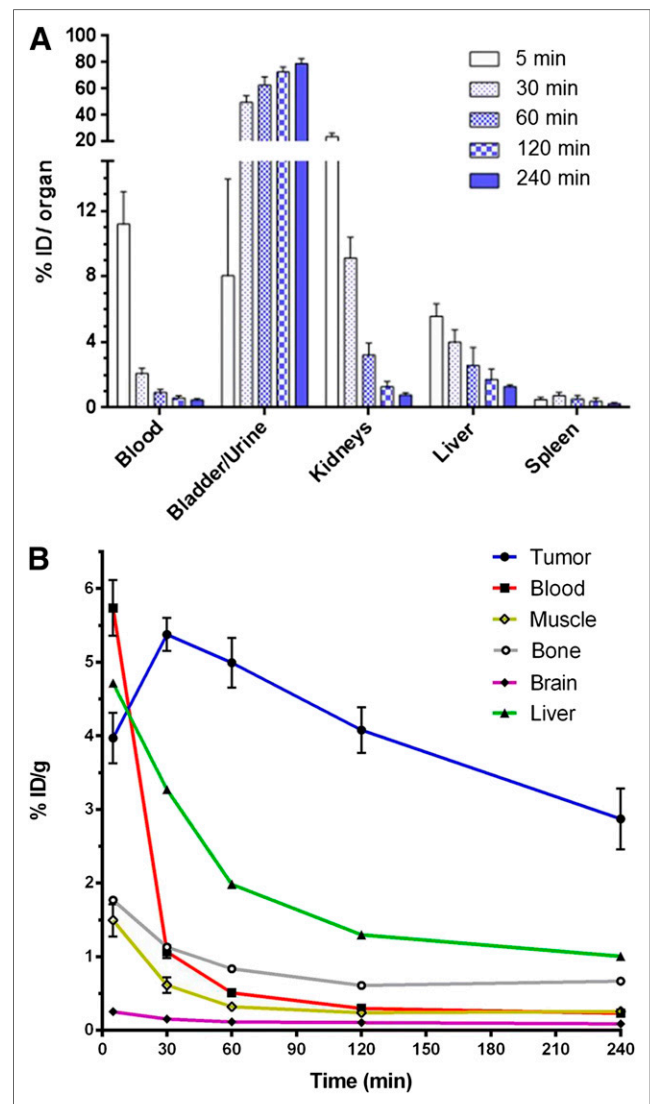

FIGURE 5. In vivo biodistribution in CD-1 nude mice bearing EL4 xenograft tumors with HPLC-purified ^{18}F-FASu. (A) ^{18}F-FASu retention in clearance organs at 5, 30, 60, 120, and 240 min after injection are shown in %ID/organ. (B) ^{18}F-FASu retention in tumor, blood, muscle, bone, brain, and liver. Data are %ID/g (mean ± SD, $n \geq 4$).

TABLE 1
Biodistribution of ^{18}F-FASu and ^{18}F-FDG in Mice Bearing Xenograft Tumors

Organ or tissue	EL4 tumors, ^{18}F-FASu	SKOV-3 tumors ^{18}F-FDG	SKOV-3 tumors ^{18}F-FASu
Blood	0.49 ± 0.12	0.58 ± 0.30	0.72 ± 0.30
Tumor	5.81 ± 1.26	1.55 ± 0.96	8.08 ± 2.03
Muscle	0.25 ± 0.16	4.92 ± 2.26	0.35 ± 0.17
Liver	1.24 ± 0.18	0.74 ± 0.15	0.86 ± 0.08
Kidney	10.11 ± 2.58	1.04 ± 0.16	15.36 ± 5.63
Spleen	4.98 ± 1.28	1.73 ± 0.59	6.74 ± 1.02
Heart	0.33 ± 0.09	54.11 ± 29.00	0.32 ± 0.07
Lungs	2.00 ± 0.38	3.61 ± 1.68	1.95 ± 0.97
Brain	0.11 ± 0.03	7.76 ± 2.77	0.09 ± 0.02
Bone	0.85 ± 0.26	3.58 ± 1.74	0.85 ± 0.53
Pancreas	23.34 ± 5.73	1.49 ± 0.54	21.19 ± 6.61
Fat	0.29 ± 0.22	0.59 ± 0.36	0.62 ± 0.67
Tumor-to-blood	12.01 ± 1.58	2.61 ± 0.27	12.08 ± 0.4.39
Tumor-to-muscle	28.16 ± 10.39	0.33 ± 0.13	29.59 ± 19.44
Tumor size	1,140 ± 296	72.60 ± 37.65	71.60 ± 39.09

Uptake values are %ID/g of tissue at 1 h after tracer injection; tumor size is in mg, mean ± SD ($n \geq 5$).

and bladder was consistent with renal clearance. Liver retention was low relative to tumor, and the bone signal cleared to less than 1 %ID/cm³, indicating that defluorination is not a prevalent metabolic pathway for ^{18}F-FASu.

DISCUSSION

^{18}F-FDG and many amino acid analog PET tracers enable detection and monitoring of tumors based on cellular metabolic changes required for sustaining cell growth and proliferation. Amino acids are needed by highly proliferative cells for anabolic protein and nucleotide synthesis and also contribute to energy metabolism by providing a carbon source for the tricarboxylic acid cycle (19). The use of amino acid analogs as PET tracers is useful, not because tumor cells increase their metabolism but rather because they enhance amino acid transport mechanisms to feed that metabolism. Here we use an L-cystine analog to target the narrow substrate profile of the cystine/glutamate transporter as a reporter of oxidative stress.

Two glutamate analogs have been reported as system x_c^- substrate PET agents, ^{18}F-FGLU and ^{18}F-FSPG (3,14). Our development strategy differed from previous reports in that we focused on a compound with similarity to the preferred uptake substrate L-cystine (9). Our lead compound, L-ASu, has an 8-atom backbone mirroring cystine while lacking a problematic disulfide bond and 1 amine to better maintain the anionic nature vital to system x_c^- substrates at physiologic pH. Indeed, we demonstrated that ³H-L-ASu was taken up more efficiently than ³H-L-Glu in our in vitro studies with SKOV-3 cells. Longer-chain anionic amino acids, such as L-ASu, have been shown to have drastically reduced affinity for metabotropic glutamate receptors (17,20); therefore, we proposed that cystine-like compounds may have a benefit of specificity over glutamate-like compounds, which are more likely to bind various glutamate receptors or use transport system X_{AG}^-. Koglin et al. reported ^{18}F-FSPG uptake in SKOV-3 tumors at approximately 3 %ID/g, whereas we demonstrated ^{18}F-FASu SKOV-3 tumor uptake of approximately 8 %ID/g at the same

time after injection. In addition, reports of preclinical and human evaluation of ^{18}F-FSPG have generally demonstrated tumor uptake similar to or less than ^{18}F-FDG (14–16). We demonstrated here that ^{18}F-FASu resulted in a 5-fold enhanced uptake over ^{18}F-FDG in SKOV-3 tumor xenografts. Further studies comparing x_c^- selectivity; glutamate receptor binding; in vitro system x_c^- uptake; in vivo biodistribution; and imaging with ^{18}F-FASu, ^{18}F-FGLU, and ^{18}F-FSPG will help evaluate differences in tracer performance. Additional comparisons with ^{18}F-FDG may reveal specific indications in which ^{18}F-FASu would be superior to or useful in addition to ^{18}F-FDG.

Activation of the gene (SLC7A11) encoding the xCT subunit of the x_c^- transport system has been reported in several cancers and cancer cell lines (10), with several groups exploring the feasibility of using the xCT transporter as a viable target for cancer therapy (10,21,22) by inducing cysteine starvation. Inhibition of the transporter reportedly restricts the growth of lymphoma (23,24), glioma (25,26), head and neck (27), breast (22), prostate (28), lung (29), and pancreatic (21,30) cancer cells both in culture and in in vivo xenograft tumors. Increased xCT transporter activity is also associated with resistance of tumors to certain types of chemotherapy, and inhibition of the xCT transporter has been shown to increase the sensitization of cancer cells to the chemotherapeutic drugs cisplatin, doxorubicin, gemcitabine, celastrol, and etoposide (27,31). Recently, a role for xCT in tumor metastatic potential has been established (32). xCT has also been linked to an undifferentiated stem-like tumor cell phenotype through its interaction with CD44 (27,33). A limited clinical study showed some success with sulfasalazine in combination with melphalan in ovarian cancer (34), whereas more recently a clinical trial has started in Japan for treatment of advanced gastric cancer with sulfasalazine (Unique Trial Number UMIN000010254). Using this transporter to image a cellular response to oxidative stress may provide functional information useful for clinical cancer care, such as detection, staging, patient stratification, and monitoring of response to therapy. If system x_c^--targeted therapies such as sulfasalazine prove efficacious in
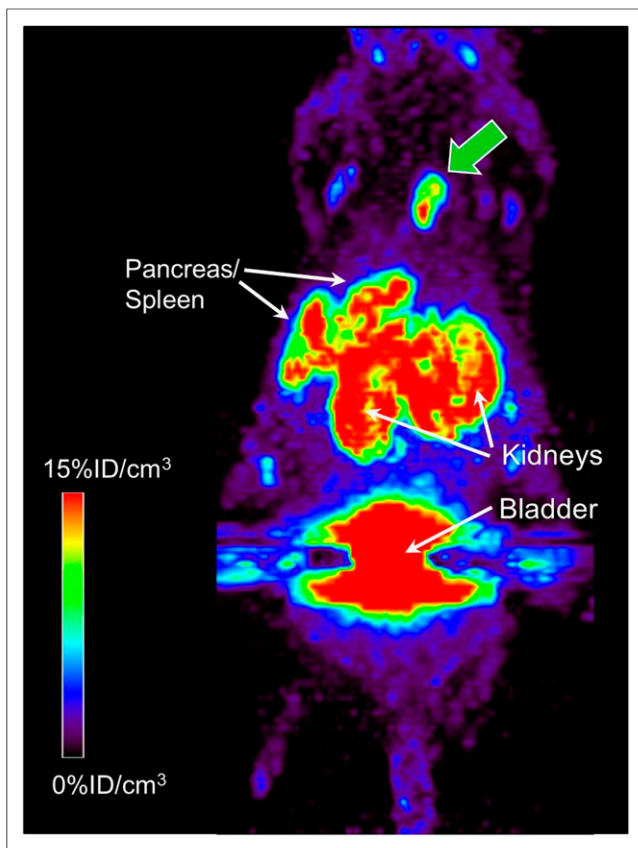
FIGURE 6. ^{18}F-FASu PET imaging in CD-1 nude mice bearing SKOV-3 xenograft tumors 1 h after injection. Maximum-intensity-projection image of 1 of 2 SKOV-3 tumor–bearing nude mice imaged in this study; tumor is indicated by green arrow. ^{18}F-FASu was HPLC-purified. On necropsy, it was determined that weight of this tumor was 31 mg.

clinical trials, companion diagnostic xCT-targeted PET tracers, such as ^{18}F-FASu, may allow stratification of patients who will respond to treatment.

Oxidative stress has also been implicated in a wide variety of pathologies other than oncology, including neurodegenerative

FIGURE 7. In vivo ^{18}F-FASu dynamic PET imaging in Rag2 M mice bearing EL4 xenograft tumor. ^{18}F-FASu was SepPak-purified. (A) PET/CT image summed over 110–120 min after injection. Tumors are indicated by arrows. (B) Region-of-interest analysis of ^{18}F-FASu uptake in tumor, liver, bone, and muscle (mean ± SD, $n = 4$).

diseases, atherosclerosis, ischemia, organ transplant rejection, autoimmune diseases, and inflammatory conditions. An xCT-targeted imaging agent such as ^{18}F-FASu may provide functional information relevant to many pathologic conditions. For example, whereas x_c^- transporter activity in the brain will provide an antioxidant defense against oxidative stress, the same mechanism appears to be complicit in neurodegeneration resulting from excitotoxic stimulation of ionotropic glutamate receptors by glutamate effluxed via system x_c^- (9,35–38). ^{18}F-FASu, ^{18}F-FGLU, and ^{18}F-FSPG are not expected to be permeable to an intact blood–brain barrier, and high basal expression of xCT is reported in normal brain. Despite this, others have reported uptake of ^{18}F-FSPG in human brain tumors (39). However, the mechanism of uptake is not clearly tumor cell–specific, because normal brain tissue uptake might be expected in regions of blood–brain barrier perturbations correlating with tumor growth or other conditions. Future studies in our group will seek to evaluate the feasibility of xCT in the brain as a potential PET tracer target.

CONCLUSION

L-ASu is taken up into cells with system x_c^- activity more readily than the natural substrate L-Glu. We have developed a novel system x_c^- substrate and demonstrated feasibility of PET imaging in SKOV-3 and EL4 tumor xenografts. ^{18}F-FASu essentially serves as a reporter for the activation of the ARE promoter, allowing functional PET imaging of a universal cellular response to oxidative stress. The mechanism of ^{18}F-FASu uptake is orthogonal to increased glucose and general amino acid uptake that is common to highly proliferative cells. ^{18}F-FASu may provide more sensitive detection than ^{18}F-FDG for certain tumor types, as was seen in SKOV-3 xenografts. Oxidative stress imaging may also find utility in determining chemotherapy resistance and as a predictor of early response to therapy.

DISCLOSURE

ACKNOWLEDGMENTS

REFERENCES

1. Neels OC, Koopmans KP, Jager PL, et al. Manipulation of [^{11}C]-5-hydroxytryptophan and 6-[^{18}F]fluoro-3,4-dihydroxy-L-phenylalanine accumulation in neuroendocrine tumor cells. *Cancer Res.* 2008;68:7183–7190.

2. Kasper BS, Struffert T, Kasper EM, et al. ^{18}Fluoroethyl-L-tyrosine-PET in long-term epilepsy associated glioneuronal tumors. *Epilepsia.* 2011;52:35–44.

3. Ploessl K, Wang L, Lieberman BP, Qu W, Kung HF. Comparative evaluation of ^{18}F-labeled glutamic acid and glutamine as tumor metabolic imaging agents. *J Nucl Med.* 2012;53:1616–1624.

4. McConathy J, Yu W, Jarkas N, Seo W, Schuster DM, Goodman MM. Radiohalogenated nonnatural amino acids as PET and SPECT tumor imaging agents. *Med Res Rev.* 2012;32:868–905.

5. Fuchs BC, Bode BP. Amino acid transporters ASCT2 and LAT1 in cancer: partners in crime? *Semin Cancer Biol.* 2005;15:254–266.

6. Bannai S, Kitamura E. Transport interaction of L-cystine and L-glutamate in human diploid fibroblasts in culture. *J Biol Chem.* 1980;255:2372–2376.

7. Okuno S, Sato H, Kuriyama-Matsumura K, et al. Role of cystine transport in intracellular glutathione level and cisplatin resistance in human ovarian cancer cell lines. *Br J Cancer.* 2003;88:951–956.

8. Valdovinos-Flores C, Gonsebatt ME. The role of amino acid transporters in GSH synthesis in the blood-brain barrier and central nervous system. *Neurochem Int.* 2012;61:405–414.

9. Lewerenz J, Hewett SJ, Huang Y, et al. The cystine/glutamate antiporter system x_c^- in health and disease: from molecular mechanisms to novel therapeutic opportunities. *Antioxid Redox Signal.* 2013;18:522–555.

10. Lo M, Wang YZ, Gout PW. The x_c^- cystine/glutamate antiporter: a potential target for therapy of cancer and other diseases. *J Cell Physiol.* 2008;215:593–602.

11. Conrad M, Sato H. The oxidative stress-inducible cystine/glutamate antiporter, system x_c^-: cystine supplier and beyond. *Amino Acids.* 2012;42:231–246.

12. Nguyen T, Nioi P, Pickett CB. The Nrf2-antioxidant response element signaling pathway and its activation by oxidative stress. *J Biol Chem.* 2009;284:13291–13295.

13. Sasaki H, Sato H, Kuriyama-Matsumura K, et al. Electrophile response element-mediated induction of the cystine/glutamate exchange transporter gene expression. *J Biol Chem.* 2002;277:44765–44771.

14. Koglin N, Mueller A, Berndt M, et al. Specific PET imaging of x_c^- transporter activity using a ^{18}F-labeled glutamate derivative reveals a dominant pathway in tumor metabolism. *Clin Cancer Res.* 2011;17:6000–6011.

15. Baek S, Choi CM, Ahn SH, et al. Exploratory clinical trial of (4S)-4-(3-[^{18}F]fluoropropyl)-L-glutamate for imaging x_c^- transporter using positron emission tomography in patients with non-small cell lung or breast cancer. *Clin Cancer Res.* 2012;18:5427–5437.

16. Baek S, Mueller A, Lim YS, et al. (4S)-4-(3-^{18}F-fluoropropyl)-L-glutamate for imaging of x_c^- transporter activity in hepatocellular carcinoma using PET: preclinical and exploratory clinical studies. *J Nucl Med.* 2013;54:117–123.

17. Bräuner-Osborne H, Slok FA, Skjaerbaek N, et al. A new highly selective metabotropic excitatory amino acid agonist: 2-amino-4-(3-hydroxy-5-methylisoxazol-4-yl)butyric acid. *J Med Chem.* 1996;39:3188–3194.

18. Julio-Pieper M, Flor PJ, Dinan TG, Cryan JF. Exciting times beyond the brain: metabotropic glutamate receptors in peripheral and non-neural tissues. *Pharmacol Rev.* 2011;63:35–58.

19. Ganapathy V, Thangaraju M, Prasad PD. Nutrient transporters in cancer: relevance to Warburg hypothesis and beyond. *Pharmacol Ther.* 2009;121:29–40.

20. Ahmadian H, Nielsen B, Brauner-Osborne H, et al. (S)-homo-AMPA, a specific agonist at the mGlu6 subtype of metabotropic glutamic acid receptors. *J Med Chem.* 1997;40:3700–3705.

21. Lo M, Ling V, Low C, Wang YZ, Gout PW. Potential use of the anti-inflammatory drug, sulfasalazine, for targeted therapy of pancreatic cancer. *Curr Oncol.* 2010;17:9–16.

22. Narang VS, Pauletti GM, Gout PW, Buckley DJ, Buckley AR. Suppression of cystine uptake by sulfasalazine inhibits proliferation of human mammary carcinoma cells. *Anticancer Res.* 2003;23:4571–4579.

23. Gout PW, Buckley AR, Simms CR, Bruchovsky N. Sulfasalazine, a potent suppressor of lymphoma growth by inhibition of the x_c^- cystine transporter: a new action for an old drug. *Leukemia.* 2001;15:1633–1640.

24. Gout PW, Simms CR, Robertson MC. In vitro studies on the lymphoma growth-inhibitory activity of sulfasalazine. *Anticancer Drugs.* 2003;14:21–29.

25. Chung WJ, Lyons SA, Nelson GM, et al. Inhibition of cystine uptake disrupts the growth of primary brain tumors. *J Neurosci.* 2005;25:7101–7110.

26. Ogunrinu TA, Sontheimer H. Hypoxia increases the dependence of glioma cells on glutathione. *J Biol Chem.* 2010;285:37716–37724.

27. Yoshikawa M, Tsuchihashi K, Ishimoto T, et al. xCT inhibition depletes CD44v-expressing tumor cells that are resistant to EGFR-targeted therapy in head and neck squamous cell carcinoma. *Cancer Res.* 2013;73:1855–1866.

28. Doxsee DW, Gout PW, Kurita T, et al. Sulfasalazine-induced cystine starvation: potential use for prostate cancer therapy. *Prostate.* 2007;67:162–171.

29. Guan J, Lo M, Dockery P, et al. The x_c^- cystine/glutamate antiporter as a potential therapeutic target for small-cell lung cancer: use of sulfasalazine. *Cancer Chemother Pharmacol.* 2009;64:463–472.

30. Lo M, Ling V, Wang YZ, Gout PW. The x_c^- cystine/glutamate antiporter: a mediator of pancreatic cancer growth with a role in drug resistance. *Br J Cancer.* 2008;99:464–472.

31. Müerköster S, Arlt A, Witt M, et al. Usage of the NF-kappaB inhibitor sulfasalazine as sensitizing agent in combined chemotherapy of pancreatic cancer. *Int J Cancer.* 2003;104:469–476.

32. Chen RS, Song YM, Zhou ZY, et al. Disruption of xCT inhibits cancer cell metastasis via the caveolin-1/beta-catenin pathway. *Oncogene.* 2009;28:599–609.

33. Ishimoto T, Nagano O, Yae T, et al. CD44 variant regulates redox status in cancer cells by stabilizing the xCT subunit of system x_c^- and thereby promotes tumor growth. *Cancer Cell.* 2011;19:387–400.

34. Gupta V, Jani JP, Jacobs S, et al. Activity of melphalan in combination with the glutathione transferase inhibitor sulfasalazine. *Cancer Chemother Pharmacol.* 1995;36:13–19.

35. Qin S, Colin C, Hinners I, Gervais A, Cheret C, Mallat M. System X_c^- and apolipoprotein E expressed by microglia have opposite effects on the neurotoxicity of amyloid-beta peptide 1-40. *J Neurosci.* 2006;26:3345–3356.

36. Savaskan NE, Heckel A, Hahnen E, et al. Small interfering RNA-mediated xCT silencing in gliomas inhibits neurodegeneration and alleviates brain edema. *Nat Med.* 2008;14:629–632.

37. Domercq M, Sanchez-Gomez MV, Sherwin C, Etxebarria E, Fern R, Matute C. System x_c^- and glutamate transporter inhibition mediates microglial toxicity to oligodendrocytes. *J Immunol.* 2007;178:6549–6556.

38. Albrecht P, Lewerenz J, Dittmer S, Noack R, Maher P, Methner A. Mechanisms of oxidative glutamate toxicity: the glutamate/cystine antiporter system x_c^- as a neuroprotective drug target. *CNS Neurol Disord Drug Targets.* 2010;9:373–382.

39. Kumar M, Mosci C, Keu KV, et al. Evaluation of the ^{18}F-labeled L-glutamate derivative ^{18}F-FSPG (BAY 94-9392) in brain and head and neck cancer patients [abstract]. *J Nucl Med.* 2012;53(suppl):274P.